

RSC Advances



This is an *Accepted Manuscript*, which has been through the Royal Society of Chemistry peer review process and has been accepted for publication.

Accepted Manuscripts are published online shortly after acceptance, before technical editing, formatting and proof reading. Using this free service, authors can make their results available to the community, in citable form, before we publish the edited article. This *Accepted Manuscript* will be replaced by the edited, formatted and paginated article as soon as this is available.

You can find more information about *Accepted Manuscripts* in the [Information for Authors](#).

Please note that technical editing may introduce minor changes to the text and/or graphics, which may alter content. The journal's standard [Terms & Conditions](#) and the [Ethical guidelines](#) still apply. In no event shall the Royal Society of Chemistry be held responsible for any errors or omissions in this *Accepted Manuscript* or any consequences arising from the use of any information it contains.

**The role of potassium chlorate on expansion of dickite layers
and the preparation of a novel TiO₂ impregnated dickite
photocatalyst using expanded dickite as carrier**

Bing Xue, Kuo Yang, Xingyuan Wang, Qianwen Chi, Yinshan Jiang*

Key Laboratory of Automobile Materials of Ministry of Education and Department of Materials Science and Engineering, Jilin University, 5988 People's Avenue, Changchun 130025, China

* **Corresponding to:** Tel: 86-0431-85094856; Fax: 86-0431-85094856.

E-mail: jiangyinshan@163.com (Y.S. Jiang)

Abstract

The layered dickite particles were expanded by rapidly heating the mixture of dickite- urea intercalation complex and KClO_3 . Then a novel TiO_2 impregnated dickite photocatalyst was prepared from the thermal hydrolysis of the expanded dickite (used as a carrier) and TiOSO_4 suspension. The resulting expanded dickite particles and the reaction mechanism were characterized by X-ray diffractometry, infrared spectroscopy, scanning electron microscopy, transmission electron microscopy, energy-dispersive spectrometry and specific surface area (SSA) test. Results showed KClO_3 reacted rapidly with the urea molecules remaining on the surfaces of the dickite-urea intercalation complex in the rapid heating. A large number of gases produced from the reaction expanded the dickite layers. The expanded layers could reach 20 nm thick and their average SSA was nearly ten times larger than that of raw dickite. The exposed inner surfaces of the expanded dickite were new places where TiO_2 particles deposited. Photocatalytic activity was evaluated by the degradation of methyl orange in aqueous solutions. The TiO_2 /dickite photocatalyst had a porous layer structure and nano-size TiO_2 particles, and demonstrated an enhanced adsorption and photocatalytic ability for the removal of methyl orange.

Keywords: dickite; potassium chlorate; TiO_2 ; photocatalyst

1. Introduction

The latest researches demonstrate that TiO_2 is recognized as the most promising semiconductor photocatalyst for purifying environment, attributing to its low cost, non-toxic and chemical/photo corrosion stability.¹⁻⁴ Nevertheless, due to the small particle size, the issues such as inactivation, aggregation, difficult separation and serious loss, severely limit the use and development of TiO_2 for the pollution treatment in the suspension system.⁵⁻⁷ As a result, a number of investigations have focused on the immobilization of TiO_2 onto glass matrix, Raschig rings, fibre optics, silica, stainless steel plates, and clay minerals.⁸⁻¹³

TiO_2 supported on inorganic clay minerals has received wide attention^{14,15}. The physical properties of clay carrier used in the suspension reactor system have to be considered. For instance, montmorillonite may be swelled rapidly in the suspension system, resulting in poor hydrodynamics.^{9,16,17} Taking into account this situation, dickite may be a suitable option.

Dickite is a clay mineral of the kaolinite group with the common chemical formula $\text{Al}_2\text{Si}_2\text{O}_5(\text{OH})_4$. It has a 1:1 layered structure, with the basic unit consisting of a SiO_4 tetrahedral sheet and an AlO_6 octahedral sheet. Dickite involves an interlayer bonding with at least 3 identifiable bonds: ionic type bonds, van der Waals forces and hydrogen bonds. These interaction forces make dickite suitable as a structurally rigid substrate for supporting and immobilizing the TiO_2 . The interaction forces also make the immobilized particles chemically stable from swelling.

Abbreviations: TiO_2/D , TiO_2 impregnated dickite; DU, dickite-urea intercalation complex; DUW, dickite-urea intercalation complex washed by anhydrous alcohol; DUH-X, calcined product of DU and KClO_3 , X was the mass proportion of KClO_3 ; DUWH-40, calcined product of DUW and KClO_3 whose mass proportion is 40 wt%; UH, calcined product of urea; KH, calcined product of KClO_3 ; UKH, calcined product of urea and KClO_3 ; DUH-40-TiO_2 , TiO_2 impregnated DUH-40 photocatalyst; D- TiO_2 , TiO_2 impregnated raw dickite photocatalyst.

For photocatalytic decomposition of a target compound, adsorption of it on the TiO₂ surface is essential prior to the surface reaction. TiO₂ supported on the substrate with higher specific surface area facilitates more effective adsorption sites than bare TiO₂.^{18,19} Therefore, the pretreatment of carrier for TiO₂ is very important to obtain higher specific surface area.

The specific surface area (SSA) of a layered clay carrier, especially clay with a 1:1 layered structure, can be effectively extended through the exfoliation or expansion of its silicate layers. For instance, kaolinite previously expanded by the intercalation of urea can be exfoliated through low-temperature washing procedures to increase its SSA from 9.4 to 20.5 m²/g.²⁰ Furthermore, the ball milling and acid treatment set before exfoliation further increase the SSA of kaolinite.²¹ Besides, different methods for exfoliation of kaolinite were reported.²²⁻²⁵ However, there are rare reports on the exfoliation or expansion of dickite. The reason is that kaolinite is the most abundant clay mineral while dickite rarely exists in the environment and has not deposited at large scale.²⁶

Our previous experiment showed that by heating a dickite-urea intercalation complex, the gases produced from the urea decomposition in the interlayer of dickite could expand the dickite layers, thus increasing the SSA of dickite powder²⁷. This dickite powder may be an alternative to support TiO₂. However, we also found the exfoliation or expansion of dickite layers was not very thorough and many dickite particles were still kept in the layered stacking state with lower SSA. If there is a chemical reagent that can promote the exfoliation or expansion of dickite layers, a suitable dickite carrier for TiO₂ with larger SSA can be obtained. The oxidant potassium chlorate (KClO₃) may be the best choice. To our knowledge, there is no investigation using KClO₃ as a promoter for preparation of higher-SSA expanded dickite or investigation using the expanded dickite as an inorganic carrier for TiO₂ in photocatalysis.

In this work, we studied the effect of KClO₃ on the expansion of dickite layers and used the expanded dickite as an inorganic carrier to synthesize a novel TiO₂ impregnated dickite photocatalyst. A series of tests were used to characterize and

evaluate the role of KClO_3 on expansion of dickite layers. The photocatalytic ability of TiO_2 /dickite was evaluated through the degradation of methyl orange (MO) in the laboratory system. The study results would provide useful information for better understanding how expanded dickite enhances the ability of the TiO_2 /dickite photocatalyst.

2. Experimental

2.1. Chemicals

KClO_3 , titanylsulfate (TiOSO_4), MO, urea, barium chloride (BaCl_2) and anhydrous alcohol were analytically pure and purchased from Shanghai Chemical Regents Co. (China). The high-purity dickite powder obtained from Chang-Bai (Jilin Province, China) was used without further purification. The dickite was dried at $110\text{ }^\circ\text{C}$ for 2 h to remove the absorbed water.

2.2. Preparation of the dickite-urea intercalation complex

The intercalation of dickite with urea was conducted following a reported procedure (2007).²⁰ The dickite powder was mixed with urea at the mass proportion of 1:1 and milled for 15 min in an agate mortar. Afterwards, the mixture was stored in a closed flask and allowed to react at $95\text{ }^\circ\text{C}$ for 48 h. The resulting product was the dickite-urea intercalation complex (DU). A part of DU samples were washed by anhydrous alcohol for three times to remove the remaining urea, and then dried at $60\text{ }^\circ\text{C}$ to evaporate the excessive ethanol. The obtained sample was noted as DUW.

2.3. Expansion of the dickite layers

The dickite was expanded as follows: DU was dry-milled, added with a certain amount of KClO_3 , and then heated. The DU-KClO_3 mixtures were milled for 15 min in an agate mortar, and then rapidly put into a $400\text{ }^\circ\text{C}$ muffle furnace to react for 5 min. The products were ground into powder in an agate mortar and denoted as DUH-X, where X was the mass proportion of KClO_3 relative to the weight of DU. For example, DUH-40 refers to the expanded dickite from the reaction of DU and 40 wt% KClO_3 . For comparison, DUW was expanded under the same conditions and the product was denoted as DUWH-X. Meanwhile, urea, KClO_3 , and the mixture of urea

and KClO_3 with the mass proportion 5:4 were also heated at the same process and were denoted as UH, KH and UKH, respectively.

2.4. Preparation of the compound photocatalyst

A TiO_2/D compound photocatalyst was prepared from the thermal hydrolysis of dickite and TiOSO_4 suspension. Typically, 2.36 g of expanded dickite (DUH-40) and 1.25 g of TiOSO_4 were dispersed in 25 ml of distilled water and magnetically stirred for 30 min. Then the mixed suspension was adjusted to pH 8.0 by adding of 15 wt% ammonia, mechanically stirred at 80 °C for 2 h, filtered and washed with distilled water. The washing was repeated several times until the washings were free from sulfate ions as indicated by BaCl_2 . The samples were dried at 120 °C for 2 h and then calcined at 500 °C for 2 h in a muffle furnace. The obtained product was the TiO_2/D compound catalyst (DUH-40- TiO_2). For comparison, another $\text{TiO}_2/\text{dickite}$ compound catalyst (D- TiO_2) was prepared from untreated dickite under the same conditions. Moreover, pure TiO_2 was also prepared for comparison.

2.5. Characterization

X-ray diffraction (XRD) study of prepared samples was performed on an X' Pert PRO diffractometer with Cu K α radiation (1.5418 Å) at 50 kV and 250 mA.

The infrared spectra (FTIR) of the samples were analyzed on a Nexus-670 FTIR spectrometer. Samples were prepared as KBr pellets.

A scanning electron microscope (SEM, JSM-6700F) equipped with EDS elemental composition analyzer and a transmission electron microscopy (TEM, JEM-1011) were employed to observe the morphology of the material at 8 kV. Before TEM observation, samples were treated by the following method. 5 mg of sample powder was dispersed in 25 ml of anhydrous alcohol. After 1 h treatment with 25kHz and 400W ultrasonic treatment, the mixed suspension was dripped on the copper network carrier. The carrier was used for TEM observation after the sample on the carrier is dry at room temperature.

Specific surface area analyses (SSA) based upon N_2 adsorption/desorption were carried out with a Micromeritics Tristar 3000 automated gas adsorption.

As representatives of organic macromolecular pollutants, methyl orange (MO) was

selected as target azo pollutant for investigating the photocatalytic effect of the catalyst. During testing, 6 mg of catalyst powder was placed into tubular quartz reactor with 10 ml of MO aqueous solution (20 mg/L). The reactor was cooled by circulating water, and placed under high pressure mercury lamp (250 W, Philips) to obtain UV-light irradiation for 20, 60, 100, 140 and 180 min. The concentration of MO in the reactor was analyzed by T6 spectrophotometer (Pgeneral, China). The supernatants were collected and analyzed at 464 nm recording the characteristic absorption peak of MO.

The UV-vis diffuse reflectance spectra (UV-vis DRS) were recorded on UV-vis spectrophotometer (UV-2550, Pgeneral, China) with an integrated sphere attachment. The analytic range was from 190 nm to 800 nm, and BaSO₄ was used as the reflectance standard.

3. Results and Discussion

3.1. Intercalation of dickite with urea

Dickite shows a typical diffraction pattern with characteristic basal reflection at 7.22 Å (Fig. 1a). The dickite-urea intercalation complexes exhibit an XRD pattern identical to that of the urea-intercalated dickite previously reported.²⁷ The d_{002} of DU and DUW is 10.68 Å (Fig. 1b,c), indicating that the interlayer distance of dickite is enlarged after the intercalation of urea. The characteristic reflections at 4.00, 2.92 and 2.83 Å in Fig. 1c belong to the unreacted urea that remains on the surface of the dickite-urea intercalation complex. After washing with anhydrous alcohol, the remaining urea is thoroughly removed and the characteristic reflections of urea disappear from the XRD pattern of DUW (Fig. 1b).

The FTIR spectra of the dickite products are shown in Fig. 2. The vibrations at 3701 and 3651 cm⁻¹ in the spectrum of raw dickite (Fig. 2a) are ascribed to the O-H stretching of inner-surface of OH of dickite, and the vibration at 3621 cm⁻¹ is attributed to the O-H stretching of inner OH.²⁷ Compared with raw dickite (Fig. 2b), the vibration band at 3622 cm⁻¹ remains the same, but the band intensities at 3701 and 3651 cm⁻¹ decrease. These results show that the OH of the interlayer surface of dickite

is disturbed by the intercalation of urea molecules. The new bands at 3387 and 3501 cm^{-1} are attributed to the formation of hydrogen bond between the NH_2 groups of urea and the oxygens of the basal tetrahedral sheet.²⁰ The formation of hydrogen bond between dickite and urea shifts the stretching frequency of urea from 3258, 1681, 1602 and 1465 to 3255, 1671, 1591 and 1477 cm^{-1} , respectively (Fig. 2b). The DU has a similar FTIR spectrum as that of DUW. There are two main differences between the FTIR spectra of DU and DUW. First, a broad vibration band appears with in 3500-3350 cm^{-1} (Fig. 2c), which is formed from the overlap of the FTIR spectra of DUW and urea in same vibration region. Second, another band exists within 1480-1450 cm^{-1} , which is caused by the adsorption effect of excessive urea on the surface of the dickite-urea intercalation complex.

3.2. Expansion of dickite layers

Figure 3 shows the XRD patterns of dickite and dickite products. On the XRD pattern of DU, the (002) diffraction ($d=10.68 \text{ \AA}$) disappears and the basal diffraction of dickite appears with d value of 7.22 \AA in Fig. 2c. The d_{002} diffraction is broader and much less intense than that of untreated dickite (Fig. 2c), indicating the degradation of dickite crystal structure along basal planes. The cause to the change in XRD pattern is attributed to the deintercalation of urea molecules from the interlayer of DU. When the samples were quickly put in the Muffle furnace at 400 $^\circ\text{C}$, the temperature is high enough to rapidly decompose urea molecules in the interlayer of DU. Ammonia gas produced by the urea decomposition expanded the dickite layers and disturbed the stacking of the ordered silicate layers, thus weakening the intensity of d_{002} diffraction.

27

When DU was mixed with KClO_3 and heated quickly at 400 $^\circ\text{C}$, the XRD patterns of calcined products changed obviously. The basal diffraction (d_{002}) of dickite is gradually weakened with the increase of the mass proportion of KClO_3 (Fig. 3d-h), and nearly disappears when the mass proportion reaches 40 wt%, indicating the stacking of disordered silicate layers (Fig. 3g). Moreover, the peaks between $2\theta = 20$ and 23° become wider and weaker in Fig. 3d-h. The broad asymmetric basal diffractions are also observed due to elastic deformation of the layers and partial

amorphization of the dickite phase during the deintercalation.²⁰ Meanwhile, an obvious diffraction peak ($d=3.16$ Å) due to KCl appears in the XRD patterns of calcined products and is intensified gradually with the increase of the mass proportion of KClO_3 (Fig. d-h). The KCl is the reaction product of KClO_3 . It is deduced that the KClO_3 may decompose at high temperature or react with other substances. No matter what reaction occurs, the significant structural transformation of dickite layers from ordered to disordered arrangement is observed from the XRD patterns. The transformation helps to form the expanded dickite particles.

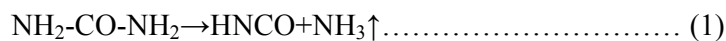
Figure 4 shows the FTIR spectra of the calcined products of DU mixed KClO_3 . The obvious characteristic hydroxyl stretching at 3701 and 3651 cm^{-1} reappears (Fig. 4c), indicating the deintercalation of urea molecules from the interlayer of DU. However, the existence of the vibration bands within 3500 - 3350 cm^{-1} and 1480 - 1450 cm^{-1} also shows the incomplete decomposition of urea molecules. When DU was mixed with KClO_3 and heated at 400 °C for 5 min, the calcined products exhibit the FTIR spectra without the characteristic vibration of urea, suggesting the complete decomposition and deintercalation of urea molecules from the interlayer of DU (Fig. 4d-h). Furthermore, the band intensities at 3701 and 3651 cm^{-1} decrease gradually with the increase of the mass proportion of KClO_3 , indicating the decrease of the interaction of hydroxyl groups. The results suggest the ordered layer arrangement along basal planes is disturbed, which is identical to the XRD analysis. Meanwhile, new bands at 3606 and 1384 cm^{-1} appear in the FTIR spectra of calcined products of DU mixed KClO_3 (Fig. 4d-h). The intensities of these bands increase gradually with the increase of the mass proportion of KClO_3 . The band at 1384 cm^{-1} is assigned to the NO_3^- vibration and the band at 3606 cm^{-1} is ascribed to N-OH vibration. The appearance of NO_3^- and N-OH vibrations suggests that nitric acid is formed in the heating process.

As indicated by SEM graphs of raw dickite (Fig. 5a), the plate-like dickite particles have a dense layer stacking morphology. The particles size is 5 - 15 μm and the thickness is 5 - 10 μm , averaged from multiple SEM images. The dickite-urea intercalation did not change the morphology of dickite (Fig. 5b), but the heating process affected the morphology significantly. As showed in Fig. 5c, the dense layer

stacking is partly expanded after the heating process. The gas produced by the urea decomposition expands the ordered layer structure. The dickite layers are further expanded when KClO_3 is used in the heating process. In the SEM graph of DUH-20, the particles in the black boxes show a like open-book-like morphology (Fig. 5d). When the mass proportion of KClO_3 reaches 40 wt%, the dickite particles are completely expanded (Fig. 5e) and the new morphology is just like accordions. Through the enlarged graph of DUH-40, the thickness of thin layers reaches 20 nm (Fig. 5f,g). These thin layers are not exfoliated and a part of them is linked together. This special morphology causes the formation of many holes and gaps, which is beneficial to the loading of the catalyst. As showed in Table 1, DUH-40 has a larger SSA than raw dickite does (48.2 vs. 4.5 m^2/g). By contrast, the layers of DUWH-40 are not completely expanded (Fig. 5h). The dickite-urea intercalation complexes without washing are beneficial to the layer expansion. In other words, the excessive urea outside the complexes is very important for expanding the dickite layers.

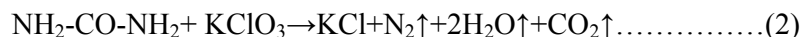
3.3. Role of KClO_3 on the expansion of dickite layers

XRD, SEM and TEM all confirm that KClO_3 can promote the expansion of dickite layers. To study the promotion mechanism, we performed some contrast experiments, with the XRD results showed in Fig. 6. Obvious characteristic diffraction of urea is observed in Fig. 6a. When heated at 400 °C, urea was transformed to cyanuric acid (HNCO), whose characteristic diffraction appears in the XRD pattern of UH (Fig. 6b). Urea underwent the following reaction:



Urea in the interlayer of DU undergoes the same reaction. The gas produced by urea decomposition escapes from the interlayer of DU and disturbs the ordered layer stacking, leading to a weak-intensity d_{002} basal diffraction in the XRD pattern of DUH-0 (Fig. 6f). Figure 6c reveals the characteristic diffraction of KClO_3 , and the XRD pattern of KClO_3 heated at 400 °C for 5 min in Fig. 6d shows little change. That means the temperature of 400 °C is not high enough to decompose KClO_3 . When KClO_3 is mixed with urea and heated at 400 °C, the reaction occurs. In the XRD pattern of the calcined product of KClO_3 and urea (Fig. 6e), characteristic diffractions

with the d value of 3.19, 2.26 and 1.83 Å belong to KClO_3 . The following reaction happened:



This is an explosive reaction that produces a large amount of gas in short time. If the reaction happens in the interlayer of dickite, it is reasonable to believe the dickite layers with close stacking will be opened up. However, there is little sign of the intercalation of KClO_3 , but KClO_3 does promote the expansion of dickite layers. Thus, there must be another reaction mechanism.

In contrast with the XRD pattern of DUH-40, the diffraction belonging to KClO_3 ($d=3.45$ and 3.34 Å) still exists in the XRD pattern of DUWH-40. Meanwhile, the characteristic diffraction of KCl does not appear in Fig. 6g. This situation suggests that KClO_3 did not react after heating when mixed with DUW. Moreover, certain reaction occurred when KClO_3 was mixed with DU because of the disappearance of KClO_3 and the appearance of KCl in Fig. 6h. The difference between DUW and DU is whether the excessive urea is washed off from the sample surfaces. For DUW, little urea on the sample surfaces can touch KClO_3 . For DU without washing, excessive urea on its surface reacts with KClO_3 , and this reaction plays an important role on expanding the dickite layers.

EDS shows the distribution of elements C and K on the sample surfaces. As showed in Fig. 7b, C is concentrated on the plane and the cross section of layered particles (the C from the surrounding conductive adhesive is ignored). The C concentration in the area where adjacent layers interconnect is a little higher than in other positions. Since C is mainly from the excessive urea in DU, its distribution represents the distribution of the excessive urea in DU. After mixing DU with KClO_3 and milling for 15 min, the element K is also distributed on the plane and the cross section of layered particles (Fig. 7d). The mixture of DU and KClO_3 shows the signals of C, O, N, Al, Si, K and Cl (Fig. 7e). When heated in the Muffle furnace, the KClO_3 and urea reacted drastically on the cross section as well as the plane of layered particles. Some urea molecules in the interlayer of DU, which were just exposed on the cross section, may also react with KClO_3 . The reaction consequence is just like to

explode many “tiny bombs” on the cross section of layered particles of DU, leading to the edge expansion of the layers. Meanwhile, the internal urea in the interlayer of DU decomposes to produce ammonia gas, which plays a synergistic effect on expanding the inside of layers. Therefore, the edge expansion from the “tiny bombs” together with the interior expansion from ammonia gas produced by urea decomposition caused the expansion of dickite layers (Fig. 8). Furthermore, XRD (Fig. 3), FTIR (Fig. 4) and SEM (Fig. 5) show that the use of more KClO₃ enhances the effect of dickite expansion. The reason is that more KClO₃ could promote a complete and sufficient reaction to create more “tiny bombs”, which are beneficial to the expansion of dickite layers. According to the FTIR in Fig. 4, nitric acid is produced in the heating process. It is indicated that another reaction between KClO₃ and urea happened:



This reaction becomes apparent when more KClO₃ is used, and thus the characteristic vibration of nitric acid is gradually intensified with the increasing proportion of KClO₃ (Fig. 4). When either reaction (2) or (3) occurs, it promotes the expansion of dickite layers.

3.4. Characterization of TiO₂/dickite photocatalyst

Figure 9 shows the crystallographic structures of pure TiO₂, D-TiO₂ and DUH-40-TiO₂. As for anatase (TiO₂), only diffraction is observed (Fig. 9a), suggesting no phase transition occurs during the preparation. The XRD pattern of D-TiO₂ (Fig. 9b) reveals the obvious characteristic diffractions of anatase TiO₂ and basal diffraction of dickite. Moreover, the characteristic diffractions of anatase TiO₂ on raw dickite are decreased slightly, indicating the carrier dickite inhibits the crystallization and crystal-growth of TiO₂.⁷ As showed in Fig. 9c, the characteristic diffraction peaks of TiO₂ become weak and wide significantly, suggesting the dickite with expanded layers exerts an apparent inhibition effect. The average crystallite sizes of pure TiO₂, D-TiO₂ and DUH-40-TiO₂ were determined from the XRD peak broadening results and the Debye-Scherrer formula to be 20.6, 19.8 and 9.5 nm, respectively (Table 1). The differences between the inhibition effects of raw dickite and expanded dickite are attributed to the different SSAs. As showed in Table 1, the

expanded dickite has a much larger SSA than raw dickite does. This is because one plate-like particle can expose more surfaces after layer expansion, thus apparently increasing SSA. When the same amount of TiO_2 is dispersed on the carriers with different SSAs, the TiO_2 contents on unit area of a carrier are different. The TiO_2 content on unit area could decrease with a larger-SSA carrier. It is not beneficial for the crystal growth, but for the improvement of the photocatalysis effect of TiO_2 . In addition, for photocatalytic decomposition of a target compound, its adsorption on the TiO_2 surface is essential prior to the surface reaction. Expanded dickite with higher SSA provides more-effective adsorption sites than raw dickite.

Figure 10 shows the TEM graphs of D- TiO_2 and DUH-40- TiO_2 . As revealed in Fig. 10a, TiO_2 particles in the agglomerated state deposit on the outer surface as well as the cross section of raw dickite. The particle size of D- TiO_2 is 120-150 nm, averaged from multiple TEM images. For DUH-40- TiO_2 , because it was dispersed via ultrasonic treatment on the copper network carrier before TEM observation, so the expanded dickite layers were destroyed by ultrasound. However, it is convenient to observe the inner surface of expanded dickite layers that is the main area for deposition of TiO_2 particles. The agglomeration of DUH-40- TiO_2 is obviously relieved and the particle size of TiO_2 is 40-90 nm (Fig. 10b).

Figure 11 shows the performance of MO decomposition under UV irradiation. Clearly, the pure TiO_2 shows lower photo-degradation ability. The photocatalytic efficiency of D- TiO_2 is enhanced, while that of DUH-40- TiO_2 is higher. Also as showed in Fig. 11, the difference of the degradation effect between D- TiO_2 and DUH-40- TiO_2 is not very obvious in the first 50 min, but becomes evident in the last 40 min. The expanded dickite with higher SSA plays an important role on improving the photo-degradation effect in the last 40 min. The MO concentration decreases gradually as the photo-degradation is prolonged and to continue the photocatalytic reaction, MO has to spread to the surfaces of the photocatalyst. The expanded dickite with higher SSA can facilitate the absorption and diffusion of MO. Therefore, at low MO concentration, DUH-40- TiO_2 exhibits higher photocatalytic rate. Figure 12 shows the performance of MO decomposition under visible irradiation. Similarly, the loaded

TiO₂ has higher catalytic ability under visible light than the unloaded TiO₂ does. Especially, DUH-40-TiO₂ shows a very high photocatalytic ability after 2 h, and the MO concentration declines linearly, which is attributed to the large SSA of the expanded dickite.

Figure 13 shows the UV–vis absorption spectra of the pure TiO₂, D-TiO₂ and DUH-40-TiO₂. The pure TiO₂ shows no absorption above its fundamental absorption edge (396 nm, Table 1). The loading of TiO₂ on expanded dickite causes a blue-shift in the absorption edge of TiO₂ (390 nm), thus offering more UV absorption. The situation may result from the higher SSA, special surface structure of expanded dickite, and size effect of TiO₂ nanoparticles. It is beneficial for enhancing the photo-degradation ability. Therefore, the photocatalytic efficiency of DUH-40-TiO₂ is higher than pure TiO₂ (Fig. 11 and Fig. 12). By contrast, the raw dickite with low SSA and without special surface structure cannot play such a role as expanded dickite.

4. Conclusions

Expanded dickite was prepared by rapidly heating the mixture of DU and KClO₃. KClO₃ reacted with the urea remaining on the DU surfaces to form many “tiny bombs”, which exploded and expanded the dickite layers in the rapid heating, while gas produced by the urea decomposition in the interlayer of DU promoted the expansion of dickite layers. The mass proportion of KClO₃ significantly affected the formation of expanded dickite, and when it reached 40 wt%, the morphology of expanded dickite particles was just like unfolded accordions. The expanded layers could reach 20 nm thick and their SSA could reach 48.2 m²/g from 4.5 m²/g of raw dickite. The expanded dickite with a porous layer structure and higher SSA was a suitable carrier to load TiO₂. The loading of TiO₂ on expanded dickite results in a blue-shift of the absorption edge of TiO₂ (390 nm), thus offering more UV absorption sites. The expanded dickite with higher SSA benefited the absorption and photocatalytic degradation of methyl orange.

Acknowledgments

Financial support from the Natural Scientific Foundation of China (Grant No.

41472035 and 51304080) and the Project of Science and Technology Department (Jilin Province, Grant No. 20140204008SF)

Notes and References

- 1 Z. W. Zhang, Y. M. Zhou, Y. W. Zhang, X. L. Sheng, S. J. Zhou and S. M. Xiang, *Appl. Surf. Sci.*, 2013, **286**, 344-350.
- 2 J. Y. Lee and W. Jo, *Ultrason. Sonochem.*, 2016, **28**, 250-256.
- 3 J. C. Bear, V. Gomez, N. S. Kefallinos, J. D. McGettrick, A. R. Barron and C. W. Dunnill, *J Colloid Interf. Sci.*, 2015, **460**, 29-35.
- 4 B. Seyghali and M. A. Zanjanchi, *P Spectrochim. Acta A*, 2015, **151**, 104-110.
- 5 Y. Cong, M. Long, Z. W. Cui, X. K. Li, Z. J. Dong, G. M. Yuan and J. Zhang, *Appl. Surf. Sci.*, 2013, **282**, 400-407.
- 6 J. Lv, T. S. Sheng, L. L. Su, G. Q. Xu, D. M. Wang, Z. X. Zheng and Y. C. Wu, *Appl. Surf. Sci.*, 2013, **284**, 229-234.
- 7 Y. Xia, F. F. Li, Y. S. Jiang, M. S. Xia, B. Xue and Y. J. Li, *Appl. Surf. Sci.*, 2014, **303**, 290-296.
- 8 J. Fernandez, J. Kiwi, J. Baeza, J. Freer, C. Lizama and H. D. Mansilla, *Appl. Catal. B-Environ.*, 2004, **48**, 205-211.
- 9 K. Mogyorosi, I. Dekany and J. H. Fendler, *Langmuir*, 2003, **19**, 2938-2946.
- 10 R. Molinari, F. Pirillo, M. Falco, V. Loddo and L. Palmisano, *Chem. Eng. Process.*, 2004, **43**, 1103-1114.
- 11 S. Takeda, S. Suzuki, H. Odaka and H. Hosono, *Thin Solid Films*, 2001, **392**, 338-344.
- 12 Z. Xiong, Y. Xu, L. Zhu and J. Zhao, *Langmuir*, 2005, **21**, 10602-10607.
- 13 W. Yan, B. Chen, S. M. Mahurin, E. W. Hagaman, S. Dai and H. Overbury, *J Phys. Chem. B*, 2004, **108**, 2793-2796.
- 14 Y. Q. Yang, G. K. Zhang and W. Xu, *J Colloid Interf. Sci.*, 2012, **376**, 217-223.
- 15 J. Liu and G. K. Zhang, *Phys. Chem. Chem. Phys.*, 2014, **16**, 8178-8192.
- 16 A. Bhattacharyya, S. Kawi and M. B. Ray, *Catal. Today*, 2004, **98**, 431-439.
- 17 H. I. Inyang, S. Bae, G. Mbamalu and S. W. Park, *J Mater. Civil Eng.*, 2007, **19**, 84-90.
- 18 A. Bhattacharyya, S. Kawi and M. B. Ray, *Catal. Today*, 2004, **98**, 431-439.
- 19 T. Torimoto, Y. Okawa, N. Takeda and H. Yoneyama, *J. Photochem. Photobiol. A: Chem.*, 1997, **103**, 153-157.
- 20 M. Valášková, M. Riedera, V. Matějka, P. Čapková and A. Slivab, *Appl. Clay Sci.*, 2007, **35**, 108-118.
- 21 M. Valášková, K. Barabaszová, M. Hundáková, M. Ritza and E. Plevová, *Appl. Clay Sci.*, 2011, **54**, 70-76.
- 22 S. Letaief, J. Leclercq, Y. Liu and C. Detellier, *Langmuir*, 2011, **27**, 15248-15254.
- 23 Y. Kuroda, K. Ito, K. Itabashi and K. Kuroda, *Langmuir*, 2011, **27**, 2028-2035.
- 24 H. A. Essawya, A. M. Youssefa, A. A. Abd El-Hakima and A. M. Rabieb, *Polym.-Plast. Technol.*, 2009, **48**, 177-184.
- 25 X. R. Zhang, J. Sun and Z. Xu, *Chinese J Inorg. Chem.*, 2005, **21**, 1321-1326.
- 26 J. Matusik, A. Gaweł and K. Bahranowski, *Appl. Clay Sci.*, 2012, **56**, 63-67.
- 27 B. Xue, P. P. Zhang, Y. S. Jiang, M. M. Sun, D. R. Liu and L. X. Yu, *J Appl. Polym. Sci.*, 2011, **120**, 1736-1743.

Table captions

Table 1 Test data of SSA value, crystallite size and absorption edge of samples

Figure captions

- Fig. 1 XRD patterns of (a) raw dickite, (b) DUW, (c) DU and (d) urea
- Fig. 2 FTIR spectra of (a) raw dickite, (b) DUW, (c) DU and (d) urea
- Fig. 3 XRD patterns of (a) raw dickite, (b) DU, (c) DUH-0, (d) DUH-5, (e) DUH-10, (f) DUH-20, (g) DUH-40 and (h) DUH-60
- Fig. 4 FTIR spectra of (a) raw dickite, (b) DU, (c) DUH-0, (d) DUH-5, (e) DUH-10, (f) DUH-20, (g) DUH-40 and (h) DUH-60
- Fig. 5 SEM micrographs of (a) raw dickite, (b) DU, (c) DUH-0, (d) DUH-20, (e,f) DUH-40, (h) DUWH-40 and TEM micrograph of (g) DUH-40
- Fig. 6 XRD patterns of (a) urea, (b) UH, (c) potassium chlorate, (d) KH, (e) UKH, (f) DUH-0, (g) DUWH-40 and (h) DUH-40
- Fig. 7 SEM photographs and EDS elemental map of (a,b, C element map) DU, (c,d, K element map) mixture of DU and potassium chlorate and EDS spectra of (e) mixture of DU and potassium chlorate
- Fig. 8 Sketch of the expansion mechanism of dickite layers
- Fig. 9 XRD patterns of (a) pure TiO_2 , (b) D- TiO_2 and (c) DUH-40- TiO_2
- Fig. 10 TEM micrographs of (a) D- TiO_2 and (b) DUH-40- TiO_2
- Fig. 11 Photocatalytic degradation of MO by pure TiO_2 , D- TiO_2 and DUH-40- TiO_2 under UV-light
- Fig. 12 Photocatalytic degradation of MO by pure TiO_2 , D- TiO_2 and DUH-40- TiO_2 under visible light
- Fig. 13 UV-vis absorption spectra of (a) pure TiO_2 , (b) D- TiO_2 and (c) DUH-40- TiO_2

Table

Table 1

Samples	SSA of carrier (m ² /g)	Crystallite size of TiO ₂ (nm)	Absorption edge of TiO ₂ (nm)
TiO ₂	---	20.6	396
D-TiO ₂	4.5	19.8	396
DUH-40-TiO ₂	48.2	9.5	390

Figure

Fig. 1

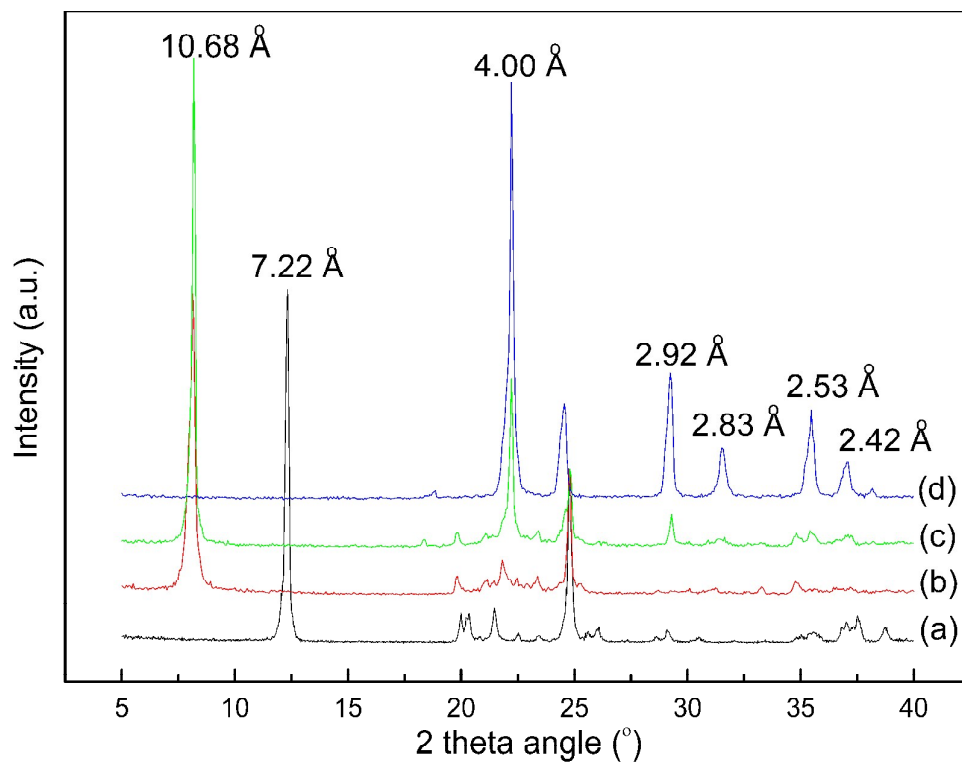


Fig. 2

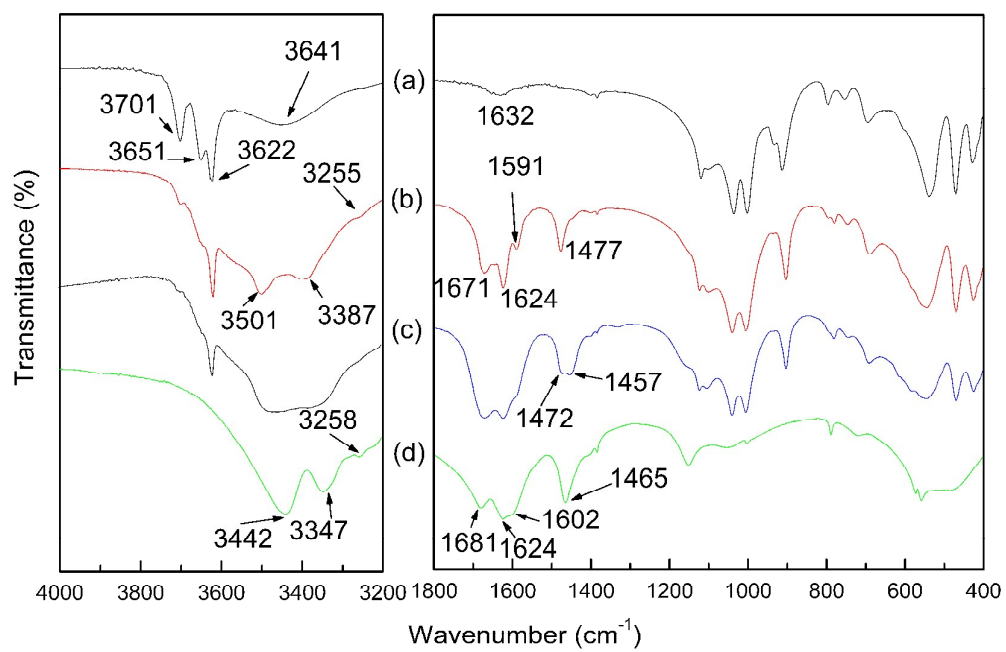


Fig. 3

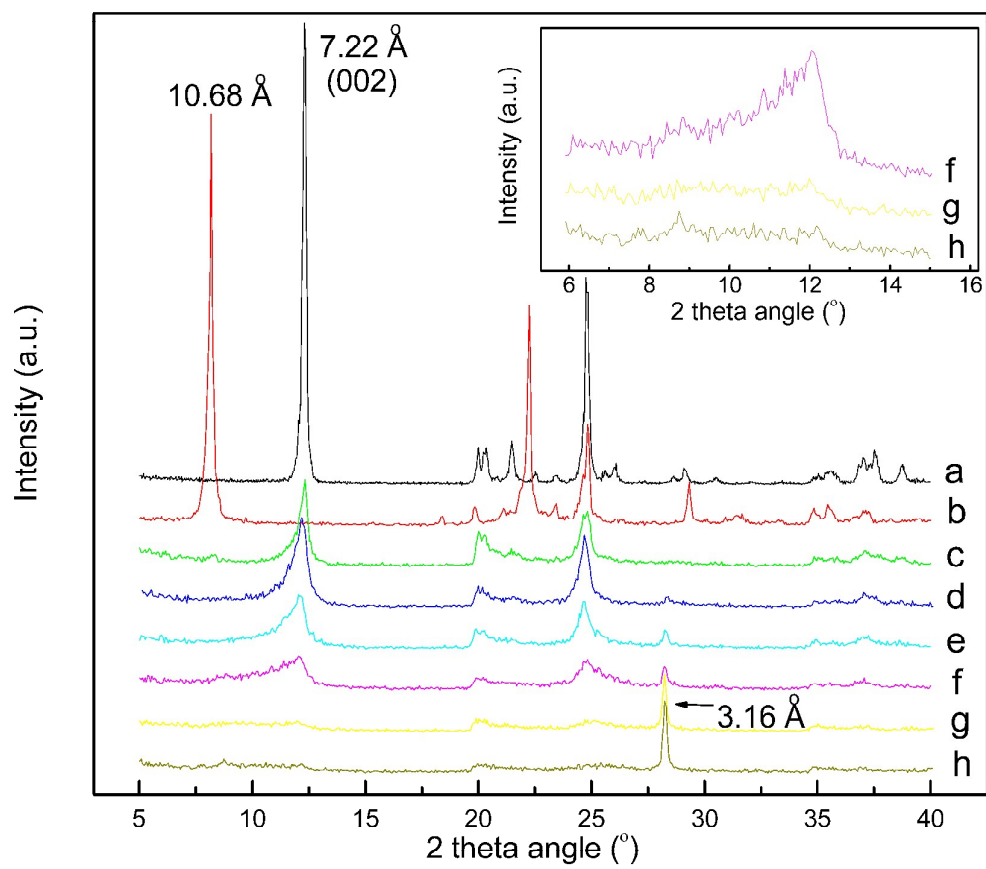


Fig. 4

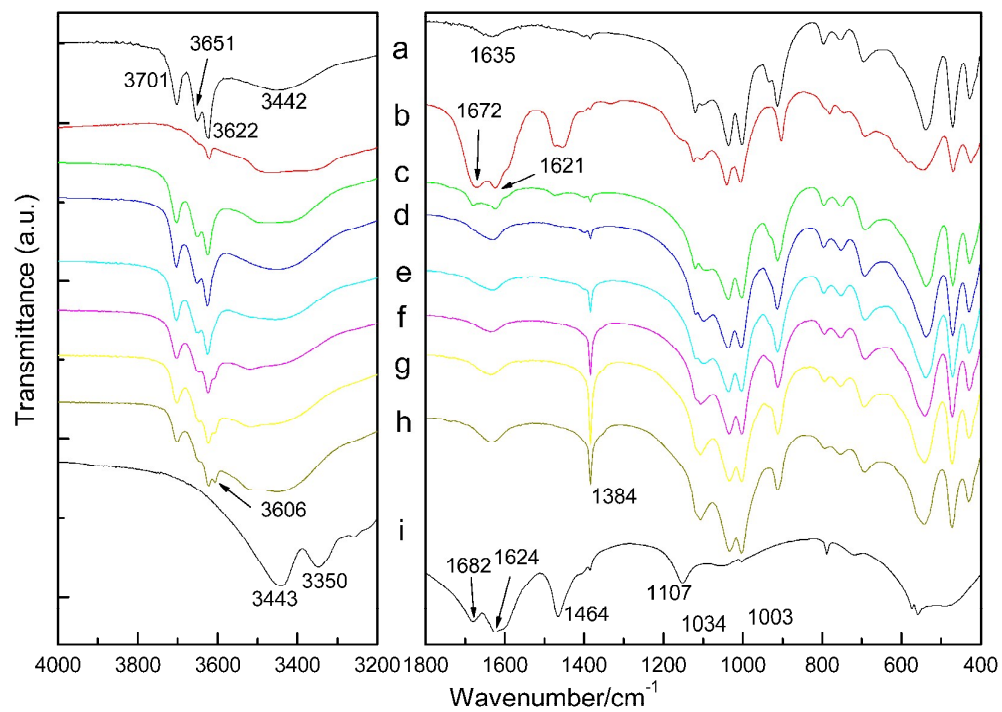


Fig. 5

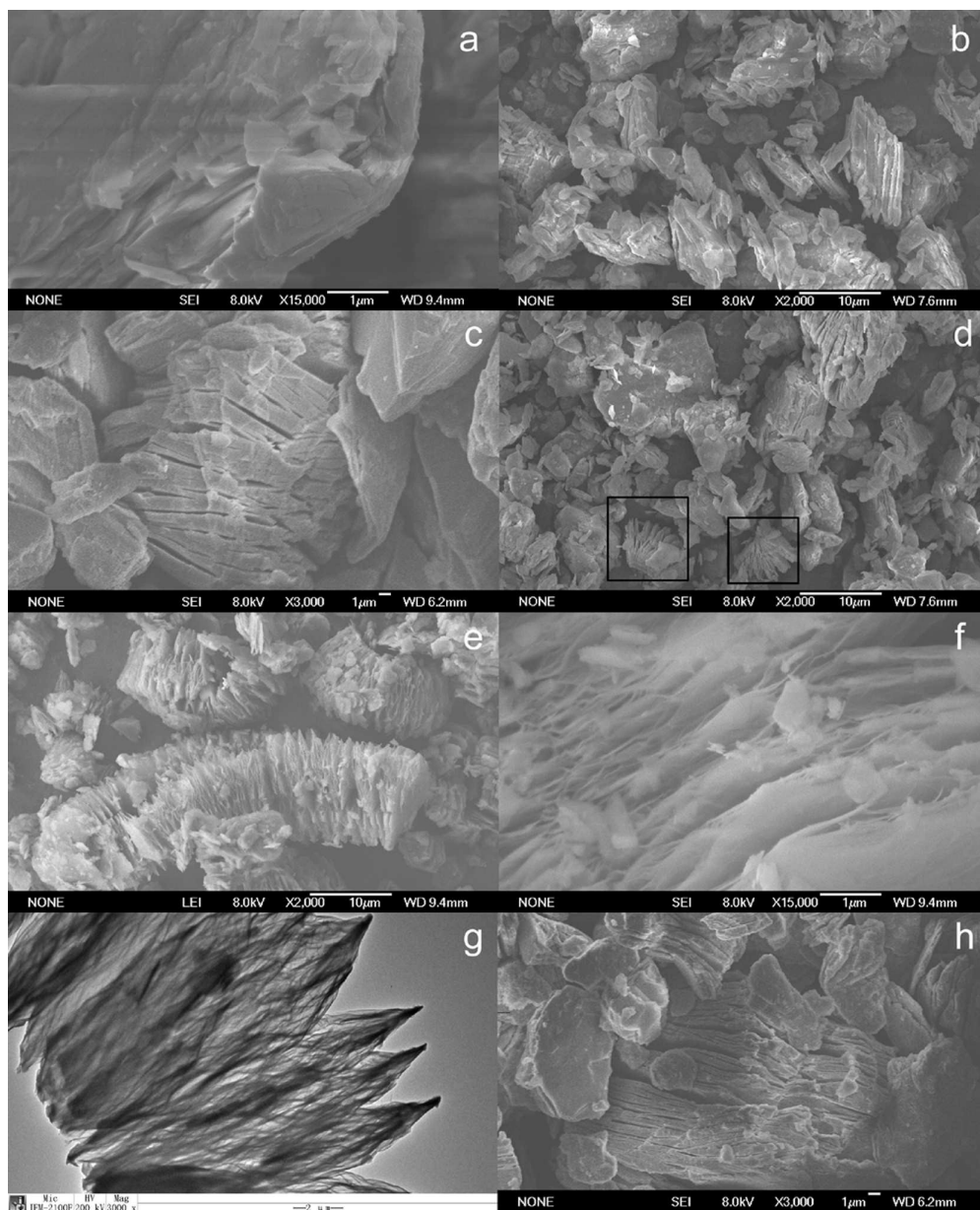


Fig. 6

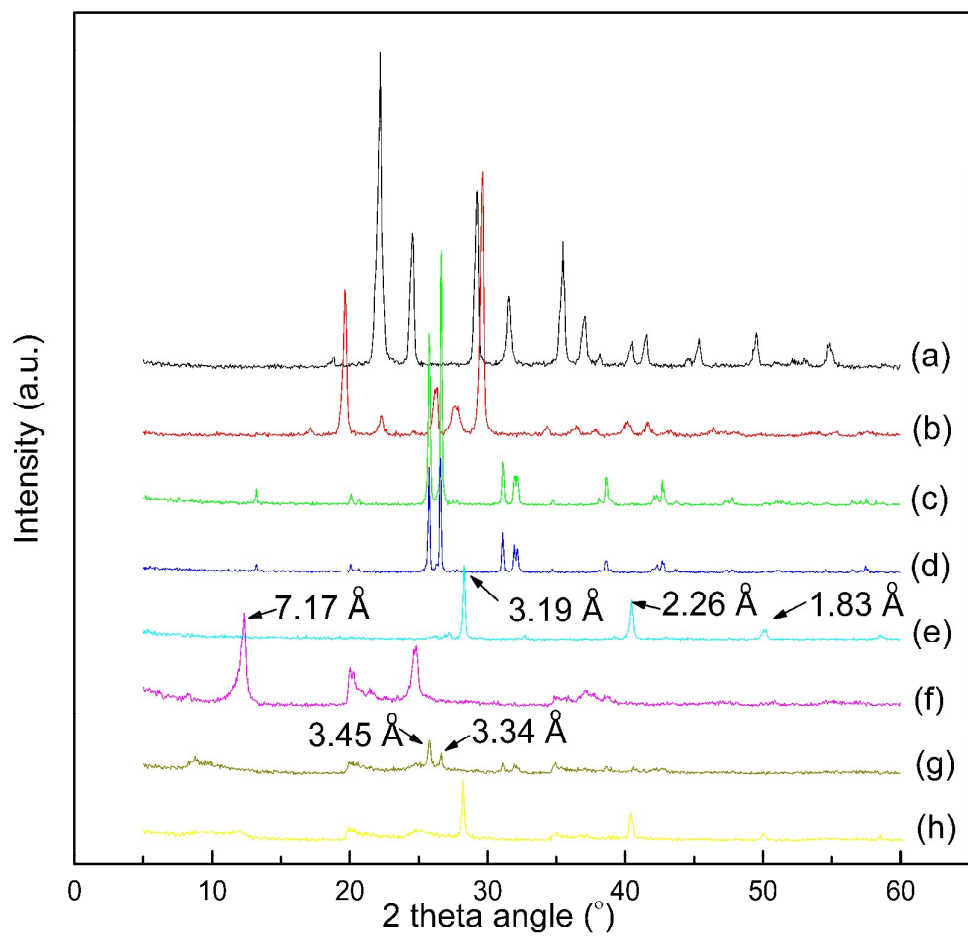


Fig. 7

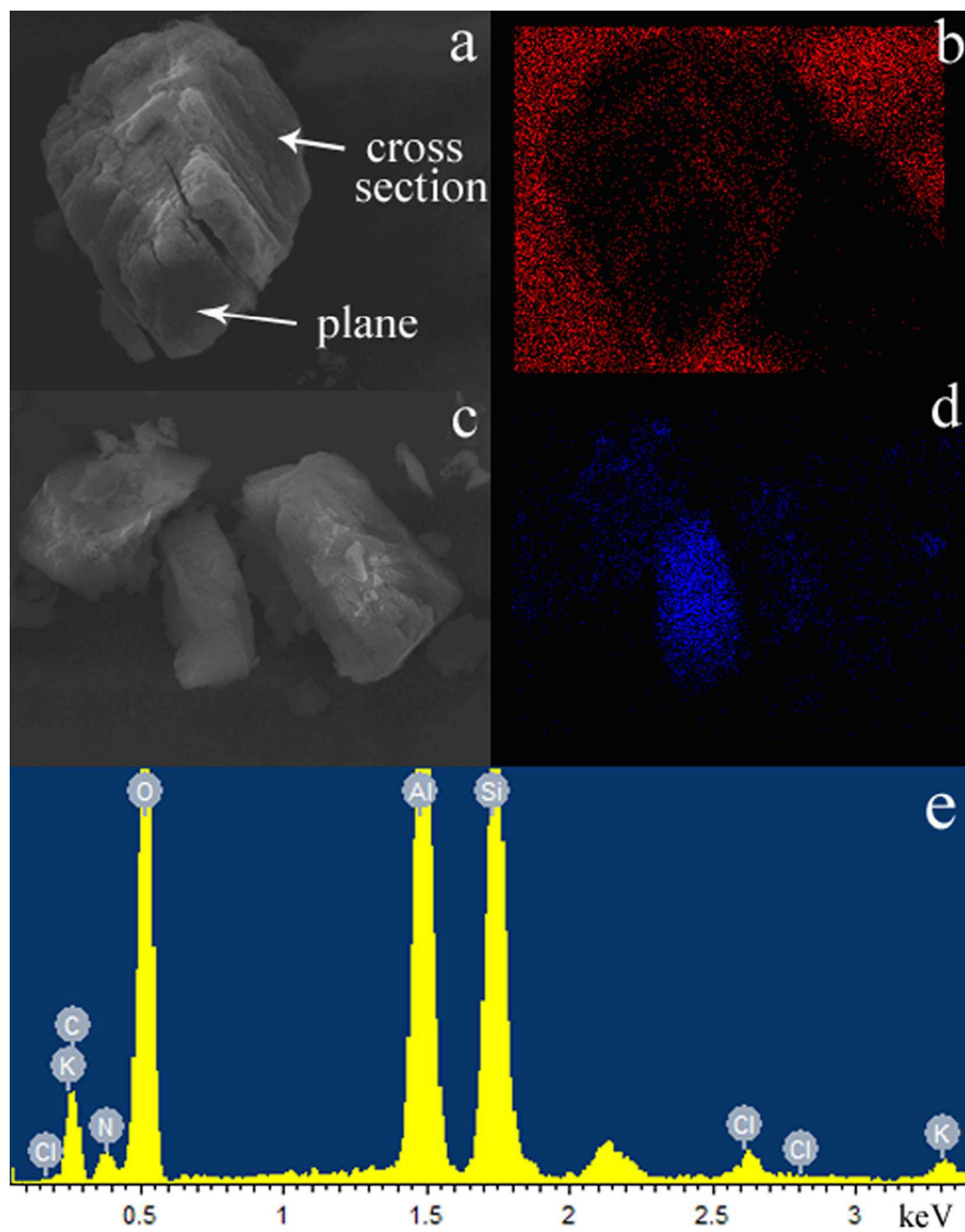


Fig. 8

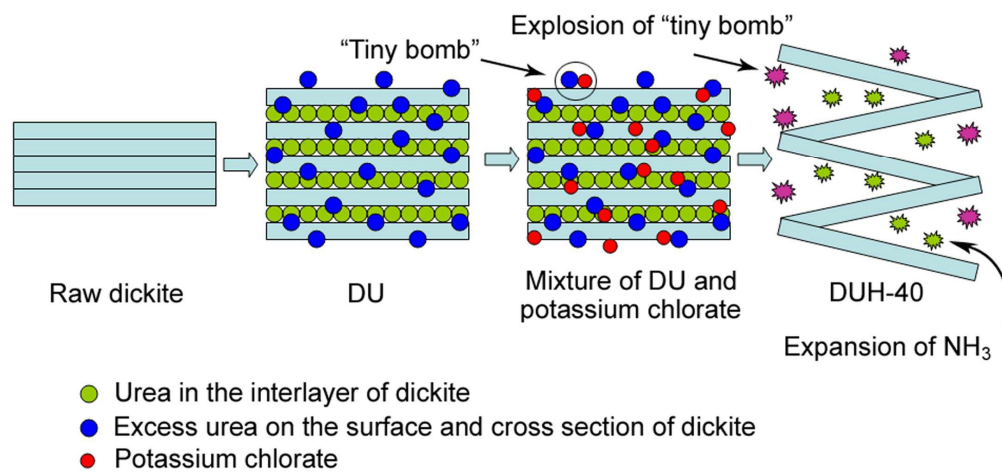


Fig. 9

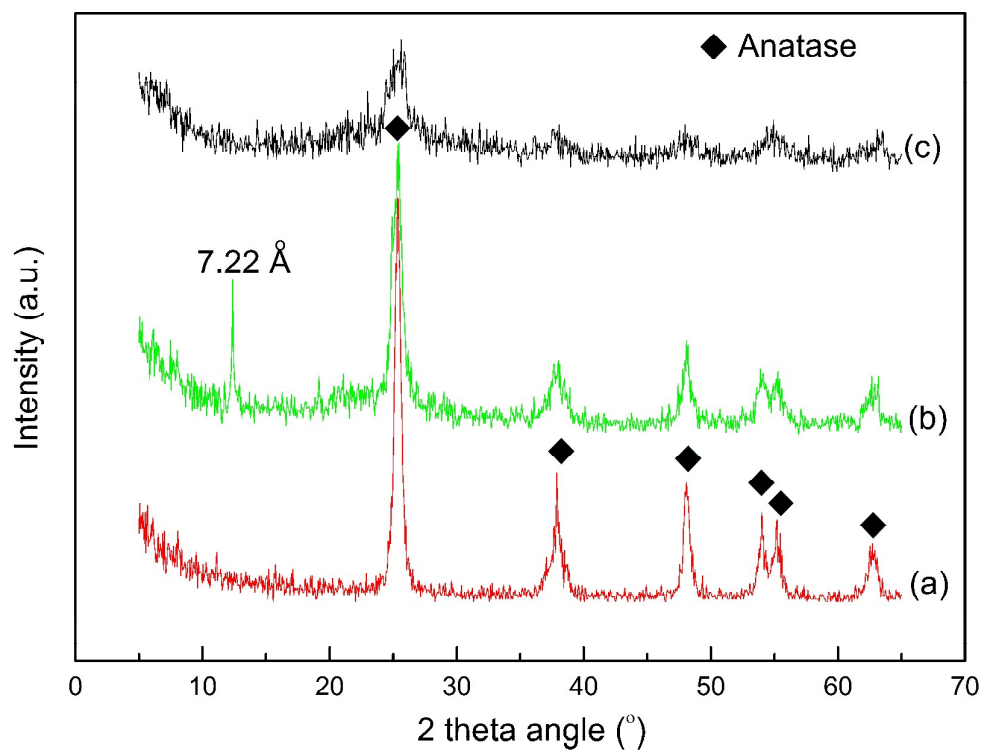


Fig. 10

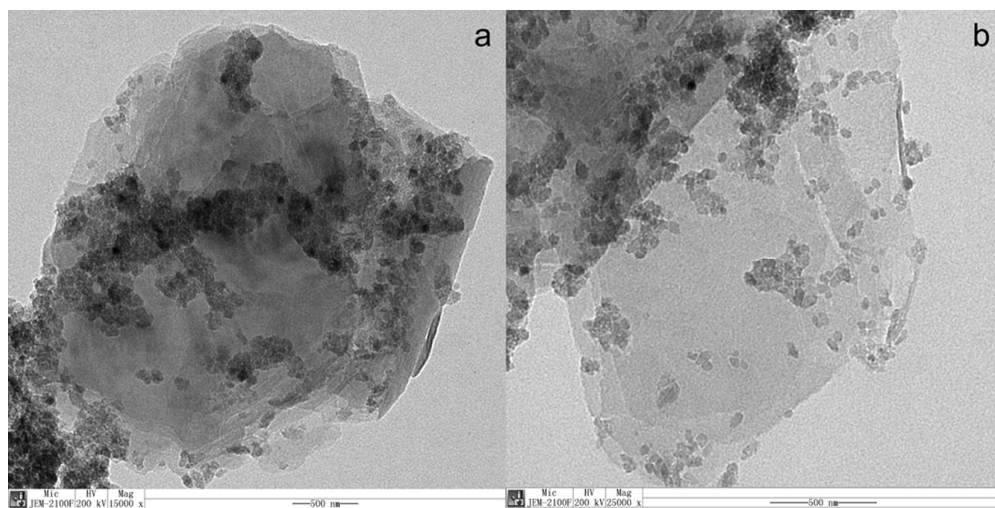


Fig. 11

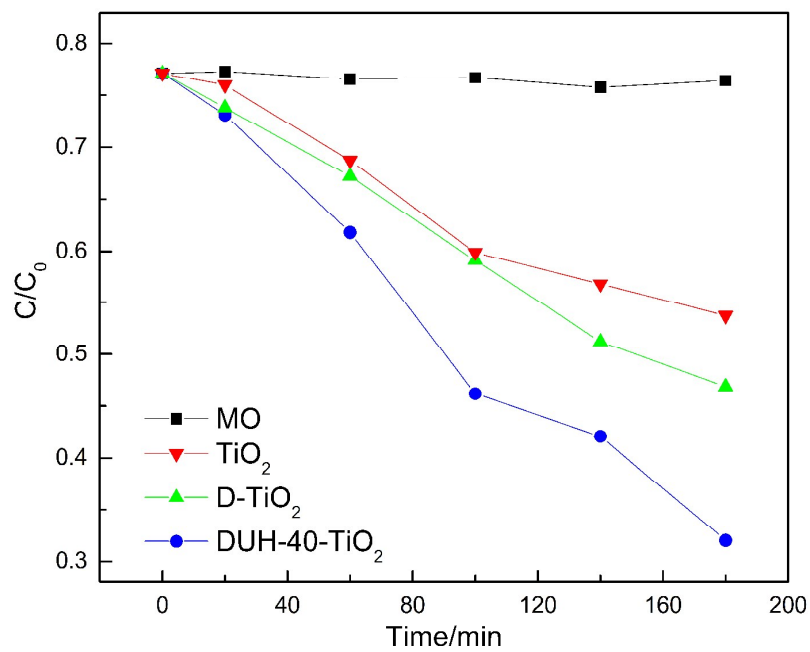


Fig. 12

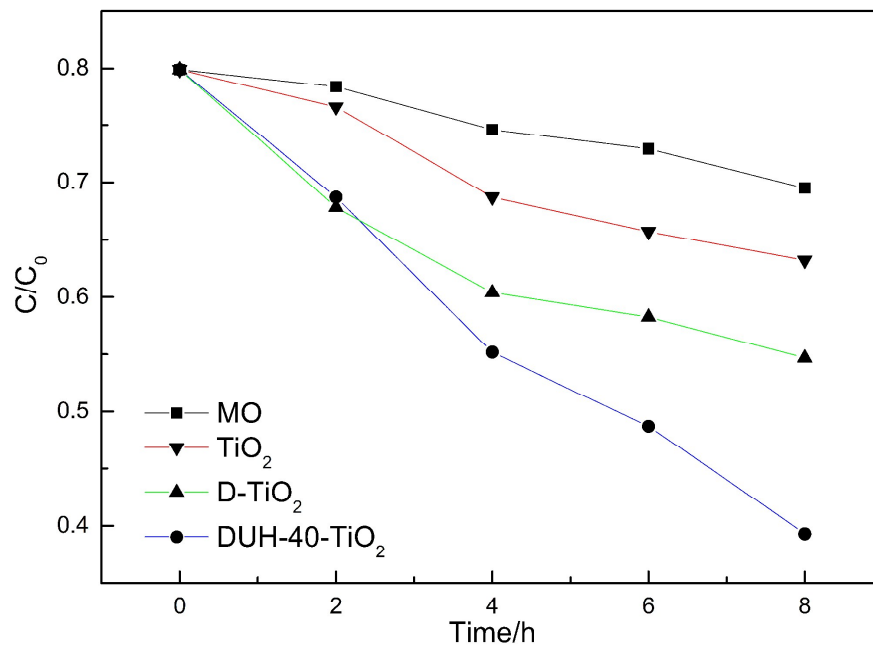
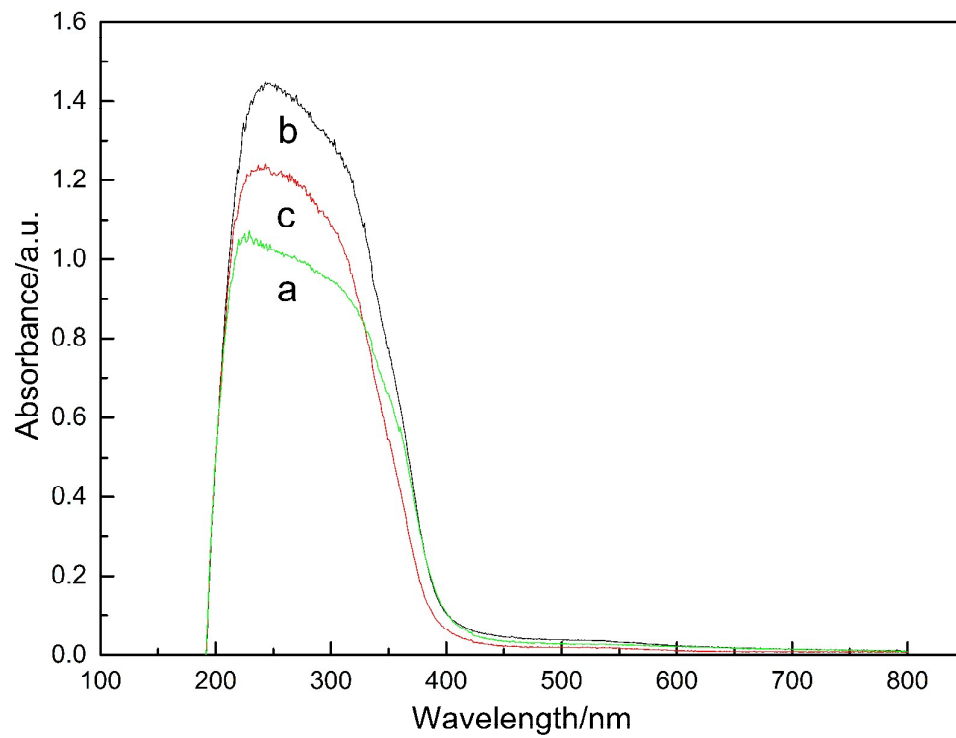
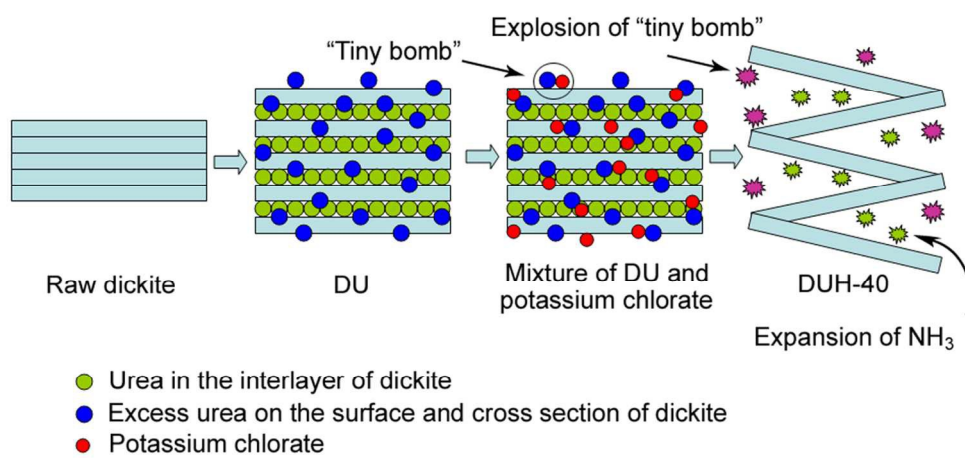


Fig. 13





351x167mm (96 x 96 DPI)